

Full color ghost imaging by using both time and code division multiplexing technologies

Le Wang(王乐), Hui Guo(郭辉), and Shengmei Zhao(赵生妹)

Citation: Chin. Phys. B, 2022, 31 (**11**): 114202. DOI: 10.1088/1674-1056/ac7e33

What follows is a list of articles you may be interested in

Full color ghost imaging by using both time and code division multiplexing technologies

Le Wang(王乐), Hui Guo(郭辉), and Shengmei Zhao(赵生妹)

Chin. Phys. B, 2022, 31 (**11**): 114202. DOI: 10.1088/1674-1056/ac7e33

Orthogonal-triangular decomposition ghost imaging

Jin-Fen Liu(刘进芬), Le Wang(王乐), and Sheng-Mei Zhao(赵生妹)

Chin. Phys. B, 2022, 31 (**8**): 084202. DOI: 10.1088/1674-1056/ac5e99

Imaging a periodic moving/state-changed object with Hadamard-based computational ghost imaging

Hui Guo(郭辉), Le Wang(王乐), and Sheng-Mei Zhao(赵生妹)

Chin. Phys. B, 2022, 31 (**8**): 084201. DOI: 10.1088/1674-1056/ac6498

Efficient implementation of x-ray ghost imaging based on a modified compressive sensing algorithm

Haipeng Zhang(张海鹏), Ke Li(李可), Changzhe Zhao(赵昌哲), Jie Tang(汤杰), and Tiqiao Xiao(肖体乔)

Chin. Phys. B, 2022, 31 (**6**): 064202. DOI: 10.1088/1674-1056/ac48f7

High speed ghost imaging based on a heuristic algorithm and deep learning

Yi-Yi Huang(黄祎祎), Chen Ou-Yang(欧阳琛), Ke Fang(方可), Yu-Feng Dong(董玉峰), Jie Zhang(张杰), Li-Ming Chen(陈黎明), and Ling-An Wu(吴令安)

Chin. Phys. B, 2021, 30 (**6**): 064202. DOI: 10.1088/1674-1056/abea8c

---

Full color ghost imaging by using both time and code division multiplexing technologies

Le Wang(王乐)[1,†], Hui Guo(郭辉)[1,2], and Shengmei Zhao(赵生妹)[1,‡]

[1] *Institute of Signal Processing and Transmission, Nanjing University of Posts and Telecommunications (NUPT), Nanjing* 210003, *China*
[2] *College of Information Engineering, Fuyang Normal University, Fuyang* 236037, *China*

(Received 20 April 2022; revised manuscript received 27 June 2022; accepted manuscript online 5 July 2022)

We propose a new full color ghost imaging scheme using both time and code division multiplexing technologies. In the scheme, the speckle patterns of three colors (red, green and blue) are modulated with different time slots and codes. The light intensity is sampled by one bucket detector. Then based on the modulated time slots and codes, we can effectively and simultaneously extract three detection component signals corresponding to three color components of objects from the sampling signal of the bucket detector. Finally, three component images resulting from the three component detection signals can be synthesized into a full color image. The experimental results verify the feasibility of our scheme under the limit of the number of time slots and codes. Moreover, our scheme reduces the number of bucket detectors and can realize high quality imaging even in a noisy environment.

Keywords: ghost imaging, time division multiplexing, code division multiplexing, full color imaging

PACS: 42.30.Va, 42.30.Wb **DOI:** 10.1088/1674-1056/ac7e33

1. Introduction

Ghost imaging (GI) is considered as an outstanding optical imaging technology,[1] which can image objects by correlating the speckle patterns with their bucket detection signals. GI was realized based on the quantum properties of entangled photon pairs by experiments in 1995.[1] Since then, GI has received considerable attention because it can be extended to the thermal light field[2–5] and has great advantages for robustness against harsh environment,[6–9] high spatial resolution[10–12] and more applications[13–16] compared to the traditional imaging technology.

Recently, constructing a full color GI scheme turns into a hot research area.[17–25] Most studies[17–19] of the full color GI have been based on use of three spectrally filtered bucket detectors, which can obtain three detection component signals corresponding to three color (red, green and blue) components of objects. Then three component images resulting from three detection component signals can be synthesized into a full color image. However, the cost of this method is high because it uses more bucket detectors than monochromatic GI, which limits its practical applications. Another method[20–25] of full color GI is based on time division multiplexing (TDM) technology (named FCGI-TDM), where the whole sampling time is divided into three recurrent time slots of fixed length, and the specific colored speckle pattern is allotted a time slot on a round-robin basis. Then three component images resulting from three time slots can be synthesized into a full color image. Hence, FCGI-TDM has the benefit of decreasing the number of bucket detectors. However, FCGI-TDM suffers from the ambient light intensity fluctuations, which degrades the imaging quality.[26]

In addition, a new full color GI with multiple input single output (MISO) technology (named FCGI-MISO)[27] is proposed to use one bucket detector to simultaneously measure three detection component signals from the speckle patterns modulated by the cosine waveforms with the specific frequency. From the perspective of code division multiplexing (CDM) technology,[28,29] the cosine waveform modulated into speckle patterns can also be regarded as a special form of modulating code. Finally, three component images resulting from three detection component signals can be synthesized into a full color image. The benefits of FCGI-MISO are that it not only requires one bucket detector to sample three component images, but also is not affected by the fluctuation of ambient light intensity. However, the realization of FCGI-MISO is limited by the number of cosine waveforms with specific frequency, especially when FCGI-MISO is extended to hyperspectral GI.

In this paper, we propose a full color GI scheme using both TDM and MISO technologies, where the speckle patterns of three colors are modulated with two time slots and two cosine waveforms of different frequencies. Because the cosine waveform modulated into speckle patterns is regarded as a special form of modulating code of CDM, our scheme can be referred to a full color GI scheme by using both TDM and CDM technologies, named FCGI-TCDM. The advantages of FCGI-TCDM are stated in the following. Firstly, it can image the object under the limit of the number of time slots and codes because FCGI-TDM with only two time slots cannot realize

†Corresponding author. E-mail: njwanglele@163.com
‡Corresponding author. E-mail: zhaosm@njupt.edu.cn

© 2022 Chinese Physical Society and IOP Publishing Ltd

full color imaging and FCGI-MISO cannot also achieve full color imaging by using only two cosine waveforms with different frequencies, however, FCGI-TCDM can achieve full color imaging by using two time slots and two cosine waveforms with different frequencies. Secondly, FCGI-TCDM can realize high quality imaging even in a noisy environment with the fluctuation of ambient light intensity. Thirdly, FCGI-TCDM reduces the number of detectors because of the requirement of only one bucket detector. In addition, FCGI-TCDM can be extended to some ghost imaging fields with one bucket detector, such as multispectral GI and polarized GI.

The organization of the paper is as follows. Section 2 presents the proposed scheme. Section 3 shows the experimental results of our scheme. Finally, we give conclusions in Section 4.

2. Scheme description

Figure 1 shows the schematic diagram of FCGI-TCDM. Three light sources with specific color in FCGI-TCDM respectively generate a uniform light field with a temporal waveform modulated by different time slots and cosine waveforms of different frequencies. Here we use two time slots ($0 < t < T/2$ and $T/2 < t < T$) and two cosine waveforms with frequencies f_1 and f_2 to realize FCGI-TCDM, where T is the time slot duration of each speckle pattern. Therefore, speckle patterns with at most four colors can be produced in FCGI-TCDM. However, because only three colored speckle patterns are required in a full color GI, we inevitably reuse one color to represent two speckle patterns. Hence, in the first time slot $0 < t < T/2$, the light from red and green sources are modulated with two cosine waveforms with frequencies f_1 and f_2, respectively. In the second time slot $T/2 < t < T$, the light from green and blue sources are modulated respectively with two cosine waveforms with frequencies f_1 and f_2. Subsequently the superposed light is modulated by a digital micromirror device (DMD) to generate a speckle pattern. Therefore, the mth speckle pattern $S^m(x,y,t)$ is

$$S^m(x,y,t) = \begin{cases} \sum_{i=1}^{2} I^m(x,y)\left[a+\dfrac{b}{2}\cos(2\pi f_i t)\right]c_i, & 0 < t < T/2, \\ \sum_{i=1}^{2} I^m(x,y)\left[a+\dfrac{b}{2}\cos(2\pi f_i t)\right]c_{i+1}, & T/2 < t < T, \end{cases} \tag{1}$$

with $I^m(x,y)$ being the spatial speckle pattern. In this paper, we use the Walsh–Hadamard speckle patterns[5] for $I^m(x,y)$. Here, a is the direct current offset of the cosine waveform; b is the cosine waveform's amplitude; $m = 1,2,\ldots,M$; M denotes the number of speckle patterns; i represents the frequency of the cosine waveforms and the color of the speckle patterns in each time slot; c_1, c_2, and c_3 represent red, green and blue, respectively.

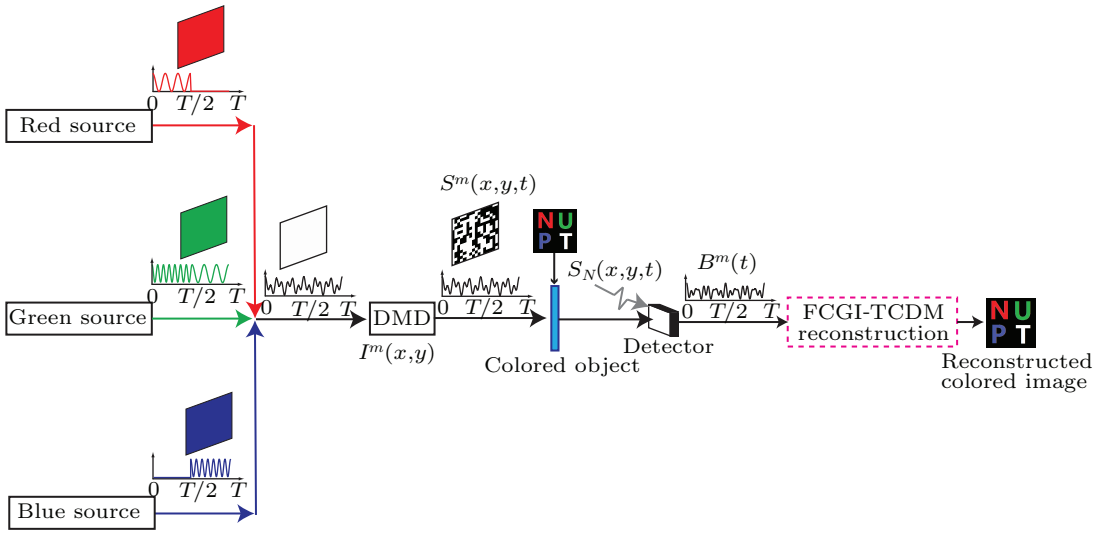


Fig. 1. The schematic diagram of FCGI-TCDM.

Then the sampling signal of the bucket detector, $B^m(t)$, is produced when the speckle patterns interacting with the object enter into the bucket detector,

$$B^m(t) = \eta \int_A [S^m(x,y,t)O(x,y) + S_N(x,y,t)]\,\mathrm{d}x\mathrm{d}y, \tag{2}$$

where η is the bucket detector's responsivity, A is the region illuminated by the speckle pattern, and $O(x,y)$ is the color object. $S_N(x,y,t)$ represents the ambient light, which can be described by[30]

$$n(t) = \eta \int_A S_N(x,y,t)\,\mathrm{d}x\mathrm{d}y = \sum_{k=1}^{\infty} n_k \cos(2\pi f_0 k t + \phi_k), \quad (3)$$

where ϕ_k and n_k are the phase and amplitude of the kth harmonic component of ambient light, respectively; f_0 is the basic frequency.

The process of the reconstruction of images is shown in Fig. 2, the sampling signal of the bucket detector $B^m(t)$ is divided into two parts in the time, which consists of the sampling signal of first time slot $B^m(t)|_{0<t<T/2}$ and the sampling signal of second time slot $B^m(t)|_{T/2<t<T}$. Then two detection component signals corresponding to red and green components of the object can be exacted from the sampling signal of first time slot $B^m(t)|_{0<t<T/2}$ by executing the Fourier transform,

$$\begin{aligned} & F\{B^m(t)|_{0<t<T/2}\} \\ &= \frac{\eta b}{4}\sum_{i=1}^{2}\int_A I^m(x,y)O_i(x,y)\,\mathrm{d}x\mathrm{d}y[\delta(f-f_i)+\delta(f+f_i)] \\ &\quad + \sum_{i=1}^{2}\eta a\int_A I^m(x,y)O_i(x,y)\,\mathrm{d}x\mathrm{d}y\delta(f) \\ &\quad + \sum_{k=1}^{\infty}\frac{n_k}{2}[\delta(f-f_0k)\,\mathrm{e}^{j\phi_k}+\delta(f+f_0k)\,\mathrm{e}^{-j\phi_k}], \end{aligned} \quad (4)$$

where $\delta(\cdot)$ represents the delta function. $F\{\cdot\}$ represents Fourier transform. $O_i(x,y) = O(x,y)c_i$ with $i = 1,2,3$ represent the red, green and blue components of the object, respectively. Hence, we can efficiently extract two detection component signals ($B^m_{1,1}$ and $B^m_{1,2}$) corresponding to $I^m(x,y)$ and the first time slot from $B^m(t)|_{0<t<T/2}$ by taking the amplitude of the Fourier transform of $B^m(t)|_{0<t<T/2}$ with specific frequency f_i,

$$\begin{aligned} B^m_{1,i} &= \left|F\{B^m(t)|_{0<t<T/2}\}_{f=f_i}\right| \\ &= \frac{\eta b}{4}\int_A I^m(x,y)O_i(x,y)\,\mathrm{d}x\mathrm{d}y, \end{aligned} \quad (5)$$

where $B^m_{1,1}$ and $B^m_{1,2}$ are red and green detection component signals in the first time slot. It is shown that FCGI-TCDM can eliminate the influence from the ambient light intensity fluctuations because the specific detection component signal can be obtained by taking the amplitude of the Fourier transform of sampling signals with a specific frequency f_i, but the noisy signal from ambient light without the specific frequency f_i will be effectively filtered.

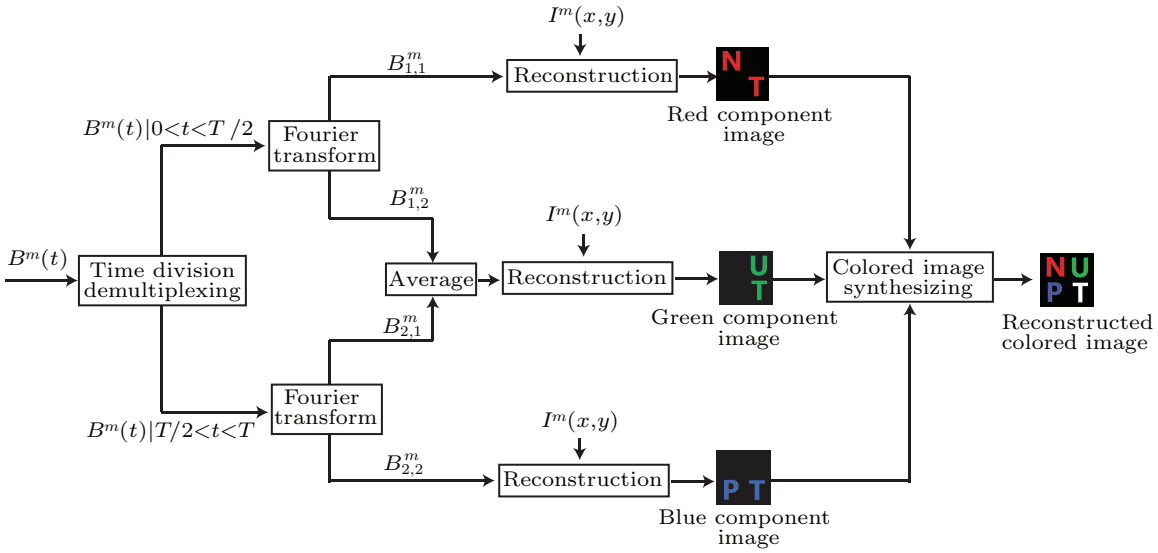


Fig. 2. The schematic diagram of FCGI-TCDM reconstruction algorithm.

Then we define that $B^m_{2,1}$ and $B^m_{2,2}$ are green and blue detection component signals in the second time slot. Similarly, two detection component signals ($B^m_{2,1}$ and $B^m_{2,2}$) can be exacted by executing the Fourier transform onto the sampling signal of the second time slot $B^m(t)|_{T/2<t<T}$,

$$\begin{aligned} B^m_{2,i} &= \left|F\{B^m(t)|_{T/2<t<T}\}_{f=f_i}\right| \\ &= \frac{\eta b}{4}\int_A I^m(x,y)O_{i+1}(x,y)\,\mathrm{d}x\mathrm{d}y. \end{aligned} \quad (6)$$

When M speckle patterns are projected onto the object and then M sampling signals are acquired by the bucket detector, we can exact the detection component signals $B^m_{j,i}|_{j=1,2;i=1,2;m=1,2,\ldots,M}$ and then the specific colored component image can be reconstructed by fast Walsh–Hadamard transform (FWHT) algorithm,[5]

$$\hat{O}_{i+j-1}(x,y) = FWHT\{B^m_{j,i}|_{m=1,2,\ldots,M}\}. \quad (7)$$

Note that the green component image can be reconstructed with either $B^m_{1,2}|_{m=1,2,\ldots,M}$ or $B^m_{2,1}|_{m=1,2,\ldots,M}$, so we use the average value of $B^m_{1,2}$ and $B^m_{2,1}$ to reconstruct $\hat{O}_2(x,y)$. Finally, the recovered three component images $\hat{O}_i(x,y)|_{i=1,2,3}$ are synthesized into a full color image $\hat{O}(x,y)$.

3. Results discussion

Figure 3 shows the experimental system of FCGI-TCDM. Three LED sources with specific color are modulated with two recurrent time slots ($0 < t < 100$ μs and 100 μs$< t < 200$ μs, where $T = 200$ μs) and two cosine waveforms with frequencies f_1 and f_2 driven by an arbitrary waveform generator (AWG, RIGOL DG812), where the amplitude and the direct current offset of the modulated cosine waveforms are $3V_{pp}$ and $3.5V$, respectively. Then, the light from three LED sources is superposed by a beam splitter, and a speckle pattern $I^m(x,y)$ is modulated onto the light by DMD (ViALUX V-7001). The speckle patterns transmitted by a TIR prism and a projecting lens are projected onto an object which is a transparent plastic thin sheet printed a colored image "fruits". Subsequently the light from the object is measured by a photodetector (Thorlabs PDA100A2) and an analog-to-digital converter (NI PCIe-6374). Note that the black box in Fig. 3 shows that a white LED driven by a Gaussian random noise waveform $n(t)$ is used as the noisy ambient light. In addition, we use mean square error (MSE)[5] to represent the difference between original image $O(x,y)$ and the reconstructed image $\hat{O}(x,y)$ with the number of pixels N, i.e., $\mathrm{MSE}(1/N)\sum_{x,y}(\hat{O}(x,y) - O(x,y))^2$.

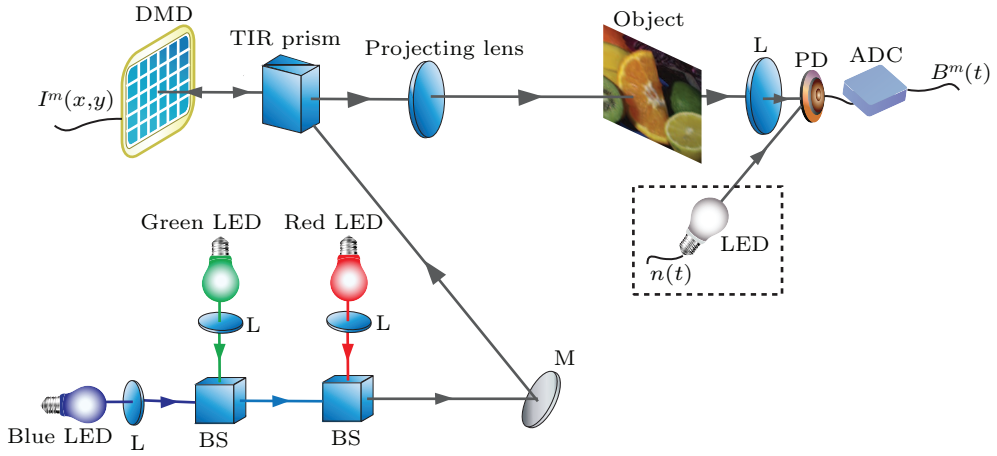


Fig. 3. The experimental system of FCGI-TCDM. LED: light emitting diode. L: lens. M: mirror. PD: photodetector. BS: beam splitter. ADC: analog-to-digital converter. TIR: total internal reflection. DMD: digital mirror device.

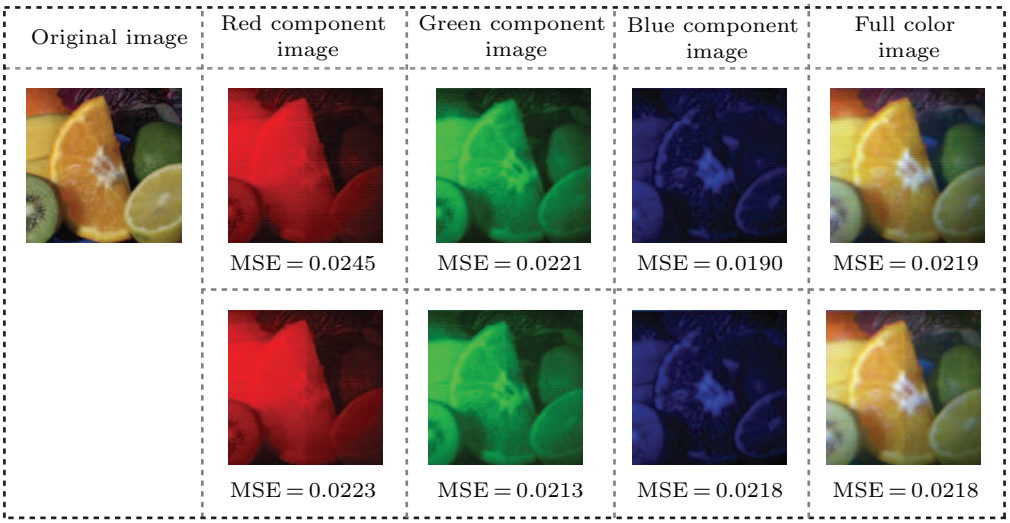


Fig. 4. The experimental results of FCGI-TCDM.

Figure 4 shows the experimental results of FCGI-TCDM to verify its feasibility. Here we use Walsh–Hadamard speckle patterns with pixel size 128×128 and $M = 16384$ in experiments. The results of FCGI-TCDM with two recurrent time slots ($0 < t < 100$ μs and 100 μs$< t < 200$ μs) and two cosine waveforms frequencies $f_1 = 170$ kHz and $f_2 = 110$ kHz are shown in the first row of Fig. 4, while the second row of Fig. 4 are the results for FCGI-TCDM with $f_1 = 120$ kHz and $f_2 = 110$ kHz. The experimental results show that the imaging quality of reconstructed three colored component images is high and the their MSEs is small. Then the synthesized full color image also has a high imaging quality. These results verify the feasibility of FCGI-TCDM. From the results in the first and second rows of Fig. 4, it is found that the

results are similar for FCGI-TCDM with different frequencies, which means that when the frequency difference between two modulated waveforms ($|f_1 - f_2|$) is not less than the minimum distinguishable frequency difference $2/T$ (note that in this paper $2/T = 10$ kHz), various detection component signals can be effectively extracted from the sampling signals. In addition, Fig. 5 shows the sampling signals of the bucket detector for the 100th speckle pattern ($B^{100}(t)$). The amplitude of the Fourier transform of the first time slot $B^{100}(t)|_{0<t<50\ \mu s}$ for modulated frequencies $f_1 = 170$ kHz and $f_2 = 110$ kHz is shown in Fig. 5(b), and then we can obtain that the red and green detection component signals are $B^{100}_{1,1} = 109.37$ and $B^{100}_{1,2} = 79.69$, respectively, from Fig. 5(b). Similarly, the amplitude of the Fourier transform of the second time slot $B^{100}(t)|_{50\ \mu s<t<100\ \mu s}$ for modulated frequencies $f_1 = 170$ kHz and $f_2 = 110$ kHz is shown in Fig. 5(c), and then we can find that the green (blue) detection component signals are $B^{100}_{2,1} = 78.85$ ($B^{100}_{2,2} = 58.11$). Moreover, for the case of modulated frequencies $f_1 = 120$ kHz and $f_2 = 110$ kHz, the red and green detection component signals obtained from Fig. 5(e) are $B^{100}_{1,1} = 112.65$ and $B^{100}_{1,2} = 66.49$, and the green and blue detection component signals obtained from Fig. 5(f) are $B^{100}_{2,1} = 78.70$ and $B^{100}_{2,2} = 57.80$.

In addition, we compare the ability of robustness against the noisy signal resulting from the ambient light intensity fluctuations among FCGI-TCDM, FCGI-TDM and FCGI-MISO. For a fair comparison, FCGI-TDM uses the three colored LED sources in turn with time slot length $T/3 = 66.7$ μs to reconstruct the corresponding colored component images. In FCGI-MISO, the sampling time for each speckle pattern is set up as $T = 200$ μs and the frequencies of the cosine waveforms for red, green and blue LED sources are 170 kHz, 110 kHz, and 230 kHz, respectively. The modulated frequencies of FCGI-TCDM are $f_1 = 170$ kHz and $f_2 = 110$ kHz. Here an LED driven by a Gaussian random noise waveform from an AWG (bandwidth 1 kHz) is used to be an ambient light. The results shown in Figs. 6, 7, and 8 demonstrate that the imaging quality of both FCGI-TCDM and FCGI-MISO will not decrease under the influence of ambient light. Even when the signal-to-noise ratio (SNR) is low, the imaging performance of both FCGI-TCDM and FCGI-MISO still does not deteriorate. The reason is that the specific colored component signal is obtained by taking the Fourier transform of the sampling signal $B_m(t)$ with a specific frequency, so these noisy signals without the specific frequency from the ambient light can be effectively filtered. Comparing to FCGI-MISO, FCGI-TCDM has the advantage that it can image the object with fewer number of codes because FCGI-MISO requires at least three cosine waveforms with different frequencies to achieve full color imaging, but only two cosine waveforms with different frequencies are used for FCGI-TCDM. The advantage of FCGI-TCDM compared to FCGI-MISO will be more significant when FCGI-TCDM is extended to multispectral GI with one bucket detector. In addition, the ambient light can obviously affect the imaging quality of FCGI-TDM. When SNR decreases, the imaging quality becomes worse and worse, and the reconstructed full color images become so blurred that one cannot see anything clearly for FCGI-TDM.

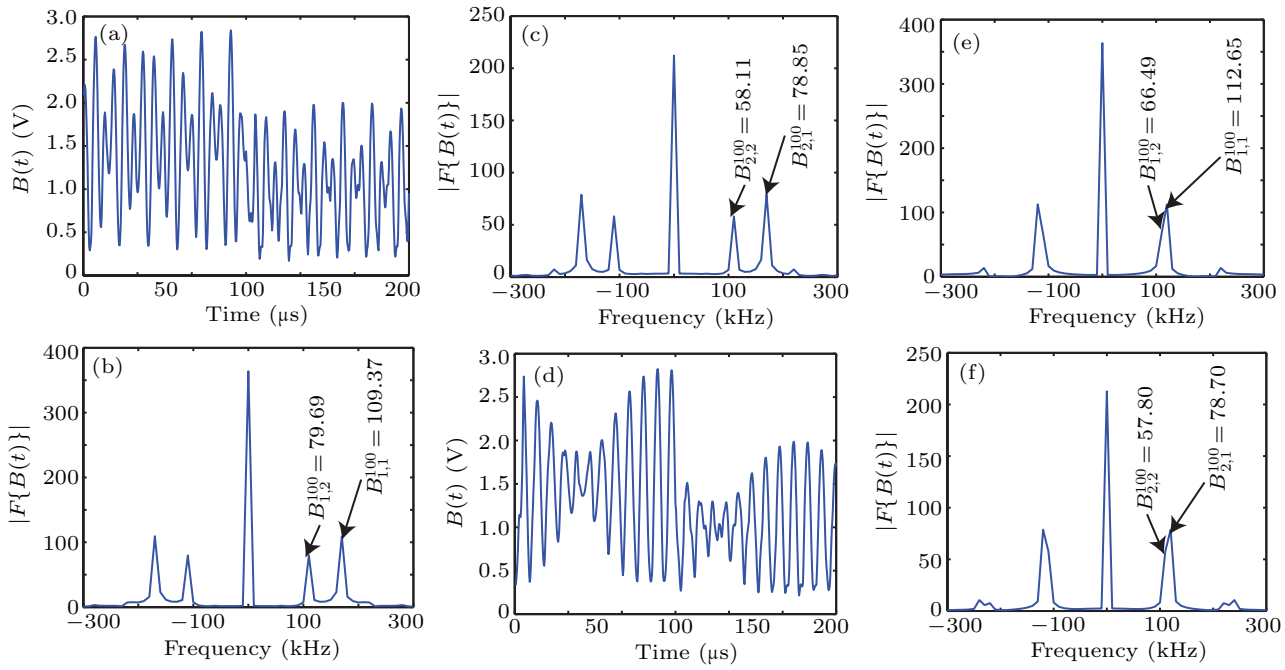


Fig. 5. (a) and (d) The sampling signals of the bucket detector for the 100th speckle pattern $B^{100}(t)$ obtained by the photodetector in experiments. (b) and (e) The amplitude of the Fourier transform of the first time slot $B^{100}(t)|_{0<t<50\ \mu s}$. (c) and (f) The amplitude of the Fourier transform of the second time slot $B^{100}(t)|_{50\ \mu s<t<100\ \mu s}$. Here, (a)–(c) give the results for $f_1 = 170$ kHz and $f_2 = 110$ kHz, and (d)–(f) show the results for $f_1 = 120$ kHz and $f_2 = 110$ kHz.

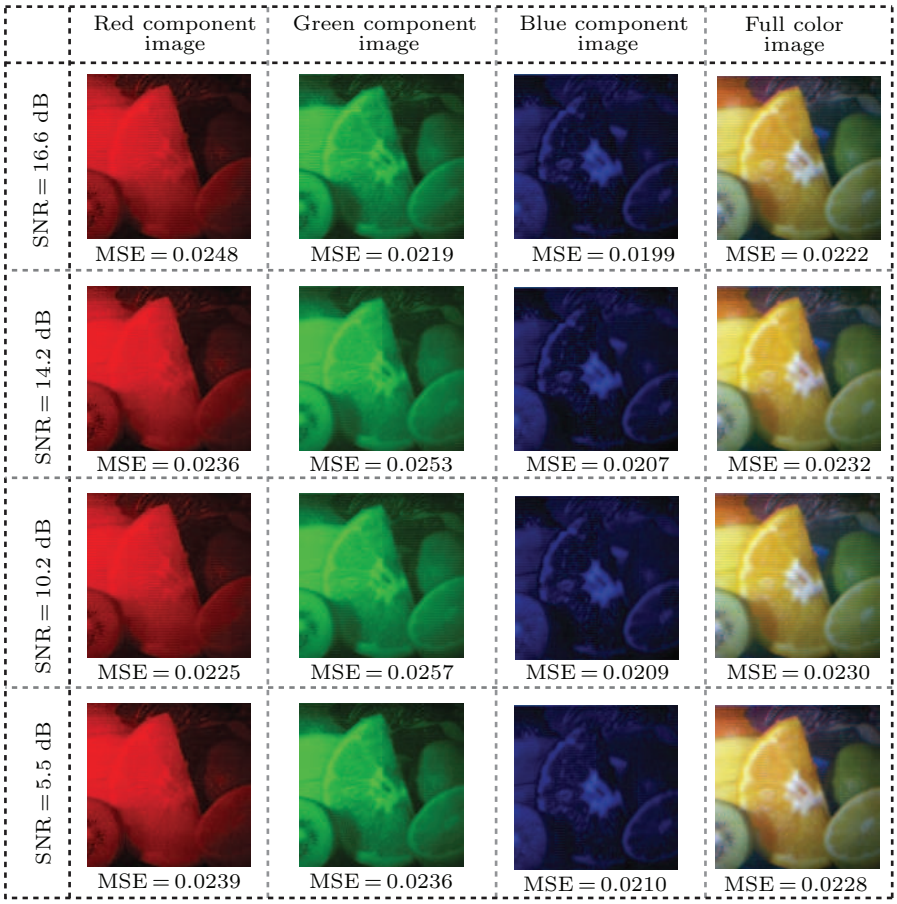


Fig. 6. The experimental results by using FCGI-TCDM with the influence of the ambient light intensity fluctuations.

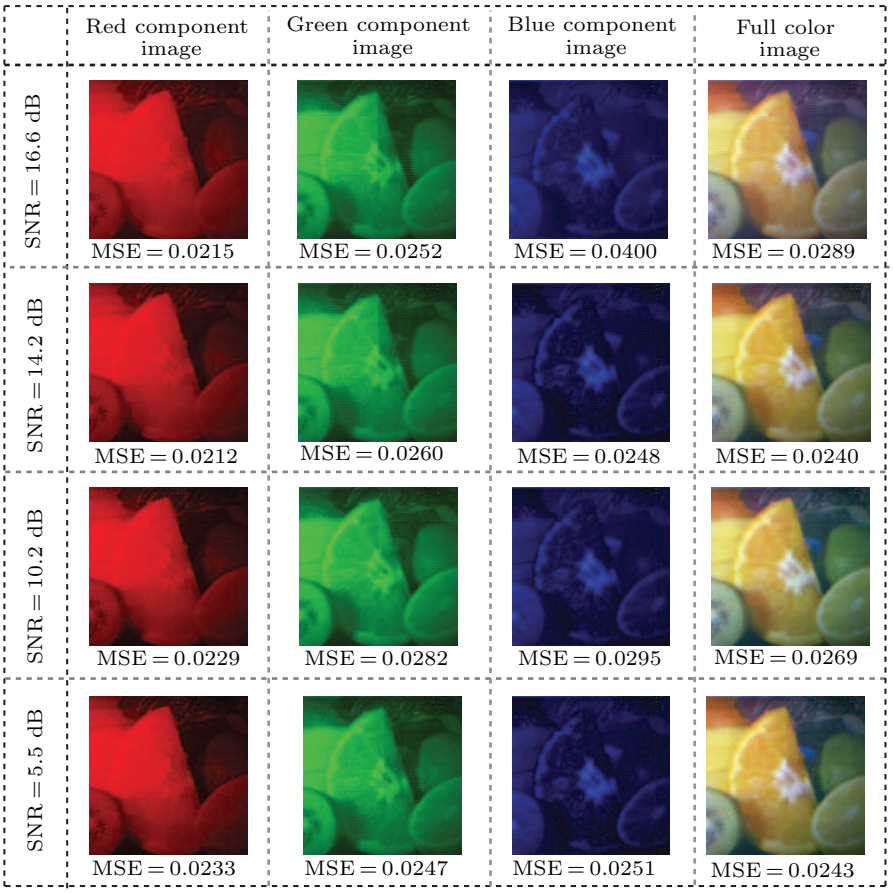


Fig. 7. The experimental results by using FCGI-MISO with the influence of the ambient light intensity fluctuations.

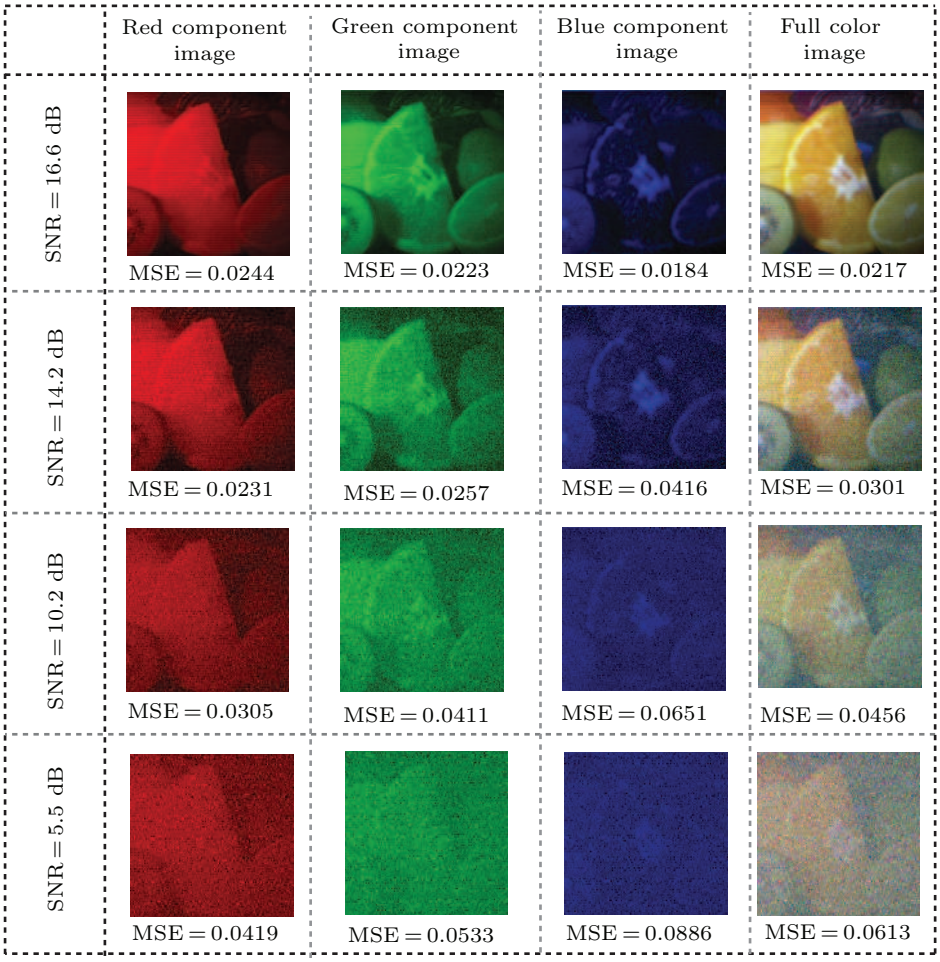


Fig. 8. The experimental results by using FCGI-TDM with the influence of the ambient light intensity fluctuations.

4. Conclusions

We have proposed a full color ghost imaging scheme using both time and code division multiplexing technologies, where the speckle patterns of three colors (red, green and blue) are modulated with different time slots and codes. The light intensity is sampled by one bucket detector. Then we can effectively and simultaneously extract three detection component signals from the sampling signal of the bucket detector based on the modulated time slots and codes. Finally, three component images are used to synthesize a full color image, where three component images can be reconstructed separately with the detection component signals and speckle patterns. We have verified the feasibility of our scheme under the limit of the number of time slots and codes by experiments. Moreover, our scheme has the advantages of the decrease of the number of bucket detectors and can realize high quality imaging even in a noisy environment.

Acknowledgements

Project supported by the National Natural Science Foundation of China (Grant Nos. 62001249 and 61871234), the NUPTSF (Grant No. NY220004), and the Scientific Research Project of College of Information Engineering, Fuyang Normal University (Grant No. FXG2021ZZ02).

References

[1] Strekalov D V, Sergienko A V, Klyshko D N and Shih Y H 1995 *Phys. Rev. Lett.* **74** 3600
[2] Bennink R S, Bentley S J and Boyd R W 2002 *Phys. Rev. Lett.* **89** 113601
[3] Shapiro J H 2008 *Phys. Rev. A* **78** 061802(R)
[4] Xu Z H, Chen W, Penuelas J, Padgett M J and Sun M J 2018 *Opt. Express* **26** 2427
[5] Wang L and Zhao S 2016 *Photon. Res.* **4** 240
[6] Deng C, Gong W and Han S 2016 *Opt. Express* **24** 25983
[7] Fu Q, Bai Y, Huang X, Nan S, Xie P and Fu X 2019 *Photon. Res.* **7** 1468
[8] Yin M Q, Wang L and Zhao S M 2019 *Chin. Phys. B* **28** 094201
[9] Wang L and Zhao S M 2020 *Chin. Phys. B* **29** 024204
[10] Wang L, Zou L and Zhao S 2018 *Opt. Commun.* **407** 181
[11] Gong W and Han S 2012 *Phys. Lett. A* **376** 1519
[12] Wang L and Zhao S 2021 *Opt. Laser. Eng.* **139** 106473
[13] Jiao S, Feng J, Gao Y, Lei T and Yuan X 2020 *Opt. Express* **28** 7301
[14] Sun S, Gu J H, Lin H Z, Jiang L and Liu W T 2019 *Opt. Lett.* **44** 5594
[15] Zhou C, Wang G, Huang H, Song L and Xue K 2019 *Opt. Express* **27** 27295
[16] Li H X, Bai Y F, Shi X H, Nan S Q, Qu L J, Shen Q and Fu X Q 2017 *Chin. Phys. B* **26** 104204
[17] Welsh S S, Edgar M P, Bowman R, Jonathan P, Sun B and Padgett M J 2013 *Opt. Express* **21** 23068

[18] Cao D Z, Xu B L, Zhang S H and Wang K G 2015 *Chin. Phys. Lett.* **32** 114208
[19] Liu B L, Yang Z H, Liu X and Wu L A 2017 *J. Mod. Opt.* **64** 259
[20] Yu W K, Yao X R, Liu X F, Li L Z and Zhai G J 2015 *Appl. Opt.* **54** 363
[21] Ye Z, Xiong J and Liu H C 2021 *Phys. Rev. Appl.* **15** 034035
[22] Salvador-Balaguer E, Clemente P, Tajahuerce E, Pla F and Lancis J 2016 *J. Disp. Technol.* **12** 417
[23] Qiu Z, Zhang Z and Zhong J 2020 *Opt. Lett.* **45** 3046
[24] Duan D, Zhu R and Xia Y 2021 *Opt. Lett.* **46** 4172
[25] Zhao Y N, Hou H Y, Han J C, Liu H C, Zhang S H, Cao D Z and Liang B L 2021 *Opt. Lett.* **46** 4900
[26] Torii T, Haruse Y, Sugimoto S and Kasaba Y 2021 *Opt. Express* **29** 12081
[27] Wang L and Zhao S 2021 *Opt. Express* **29** 24486
[28] Goldsmith A 2005 *Wireless Communications* (Cambridge: Cambridge University Press)
[29] Liu J, Wang L and Zhao S 2021 *Opt. Express* **29** 41485
[30] Moreira A J C, Valadas R T and de Oliveira Duarte A M 1997 *Wireless Networks* **3** 131